American Journal of Engineering Research (AJER)

e-ISSN: 2320-0847 p-ISSN: 2320-0936

Volume-14, Issue-10, pp-54-71 www.ajer.org

Research Paper

Open Access

A Coupled Probabilistic-Physical Framework for Slope Stability Under Hydrological Forcings in Reservoir Water-**Level Fluctuation Zones**

Guang-Xin Zhang 1,3 · Zi-Chao Shen2 * · Li-Wen Qiu 1,3 · Gui-Yun Huang 1,3 · Di Wu 1, ³·Shi-Jiang Zhu ²

- 1. National Engineering Research Center of Eco-Environment Protection in the Yangtze River Economic Belt, Wuhan 430014, China
- 2. Hubei Key Laboratory of Hydropower Engineering Construction and Management, China Three Gorges University, Yichang, 443002, China
- 3. Hubei Key Laboratory of Rare Resource Plants in Three Gorges Reservoir Area, Yichang, Hubei 443000, China

Abstract

The stability of bank slopes in the Three Gorges Reservoir's water-level fluctuation zone (WLFZ) is threatened by the dynamic and coupled impacts of rainfall and reservoir operations, yet the hydro-triggering mechanisms remain insufficiently quantified. To address this gap, this study develops an integrated probabilistic-physical framework to assess slope failure probability under complex hydrological forcings. The framework constructs a trivariate Copula-based joint distribution to capture the non-linear dependencies among rainfall intensity (I). duration (D), and reservoir fluctuation rate (R), and couples it with a finite element slope model to derive the Critical Rainfall Pattern Curve (CRPC), which quantifies hydrological thresholds for instability. Results indicate that the Gaussian Copula effectively reproduces the strong lower-tail dependence between rainfall and drawdown, demonstrating that frequent moderate disturbances dominate cumulative risk. Both vegetation reinforcement and the combined vegetation-drainage system elevate the CRPC markedly, with the synergistic measure outperforming standalone protection—reducing the single-event failure probability (P_{Fl}) by 4 % and the annual failure probability (P_{EL}) by 42%. Long-term risk evolution analysis further reveals that although P_{EL} grows non-linearly with event frequency, the lifetime probability $(P_{\scriptscriptstyle FM})$ approaches certainty within typical design lives, underscoring that reducing annual risk is pivotal for sustaining long-term slope safety. Overall, the proposed framework provides a robust quantitative tool for dynamic risk assessment, early-warning applications, and eco-engineering optimization in the WLFZ and other regulated reservoir systems.

Keywords Water-level fluctuation zone Bank slope stability Copula function Vegetation protection

Date of Submission: 08-10-2025 Date of acceptance: 19-10-2025

I. Introduction

The operation of the Three Gorges Reservoir has created a periodic water-level fluctuation zone (WLFZ) with a vertical range of 30 meters, covering a total area of 348.93 km² (Zhang et al. 2022). The geomaterials of the bank slopes in this region are persistently subjected to the alternating disturbances of unsteady reservoir water-level fluctuations and intense rainfall. This leads to frequent wet-dry cycles, which in turn induce the structural degradation of the rock and soil mass. Consequently, this degradation results in reduced shallow shear strength, vegetation decline, and diminished ecological stability, causing geohazards such as landslides to become increasingly frequent (Wang et al. 2020; Jian et al. 2018), posing a significant threat to the shipping safety of the Yangtze River and the ecological stability of the reservoir area.

Substantial progress has been made in the study of reservoir bank slope stability. Through field monitoring, physical experiments, and statistical methods, some scholars have identified intense rainfall and reservoir water-level fluctuations as typical triggering factors. They have also established critical threshold models, such as the widely used Intensity-Duration (I-D) relationship, providing a crucial theoretical basis for elucidating landslide triggering mechanisms (Demisa et al. 2025; Liu and Wang 2023; Guzzetti et al. 2008).

However, most existing studies are still constrained by certain limitations. The majority of models are either driven by a single hydrological factor or employ extreme events as standalone boundary conditions. Such approaches are inadequate for revealing the synergistic failure mechanisms arising from the interplay between rainfall and water-level fluctuations, nor can they capture their complex statistical dependence structure. Specifically, in the Three Gorges Reservoir, a rapid water-level drawdown abruptly alters the stress field and seepage regime of the bank slopes, significantly undermining their initial stability and increasing their susceptibility to low-to-moderate intensity rainfall (Zhao et al. 2017). The hazardous effect of this "dangerous combination"—a non-extreme rainfall event superimposed on a rapid drawdown—far exceeds the predictive capabilities of traditional single-factor models (Hou et al. 2022).

Furthermore, prevailing models often assume that hydrological factors are statistically independent or linearly correlated. This assumption fails to capture the complex statistical features commonly observed in nature, such as non-linear, asymmetric, and tail dependencies, leading to a systematic underestimation of the joint occurrence probability of such combined scenarios. Therefore, there is an urgent need to develop a new analytical framework that integrates the multivariate joint probability structure of triggering factors with the physical failure response process. Such a framework would provide a more scientific basis for the dynamic risk assessment and protection design of bank slopes in water-level fluctuation zones.

To comprehensively elucidate the multi-factor synergistic failure mechanism of bank slopes in the water-level fluctuation zone, this paper proposes a coupled probabilistic-physical analytical framework. The core innovations of this framework are threefold: First, regarding the characterization of triggering factors, the framework introduces multivariate joint modeling techniques to precisely capture the non-linear dependencies among key variables such as rainfall intensity (I), duration (D), and the rate of water-level change (R). This allows for the quantification of the true occurrence probability of various combined scenarios. Second, in terms of physical response simulation, a responsive slope model is developed to systematically evaluate the physical failure process under different hydrological scenarios. The model also incorporates engineering and ecological factors to identify their risk-modulating mechanisms. Finally, within the risk assessment system, the integration of the probabilistic and physical models establishes a complete conversion chain from "hydrological scenario drive" to "risk probability output". This provides quantitative support for comparing and optimizing the effectiveness of different protective measures. This study takes a typical bank slope in the water-level fluctuation zone of the upstream Three Gorges Reservoir as a case study. Utilizing measured hydrological data and in-situ parameters, we conduct a systematic analysis encompassing hydrological factor identification, stability modeling, and an evaluation of the effectiveness of protective measures. The research aims to deepen the scientific understanding of non-steady-state failure mechanisms in bank slopes and to provide a robust theoretical basis and methodological support for landslide risk warning and the optimal design of eco-protection engineering.

II. Study Area and Data Sources

This study was conducted from March 2024 to June 2025 at the Xiakou Test Base in the Three Gorges Reservoir area (110.7°E, 31.1°N). The Xiakou Test Base is located in Xiakou Town, Xingshan County, Yichang City. As one of the key bank sections of the Three Gorges Reservoir area, its bank slope stability is directly related to the safe operation of the Three Gorges Project and the safety of the lives and property of the people in the reservoir area.

The study area has a subtropical monsoon climate, with a mean annual temperature of approximately 16.9°C and a high mean annual precipitation of 1100 mm, concentrated predominantly in the summer months. As a core area affected by the Three Gorges Reservoir, the bank slopes are subjected to periodic water-level fluctuations with a vertical range of nearly 30 meters each year. This strong anthropogenic intervention, primarily driven by reservoir regulation, couples with the region's intense rainfall to form the principal driving force behind bank slope instability (Jian et al. 2014). The fluvial island in the Tongzhuang River was specifically chosen as the study site to precisely capture the slope failure risk under the dual effects of "natural rainfall and artificial regulation" and to validate the multivariate probabilistic analysis framework proposed herein.

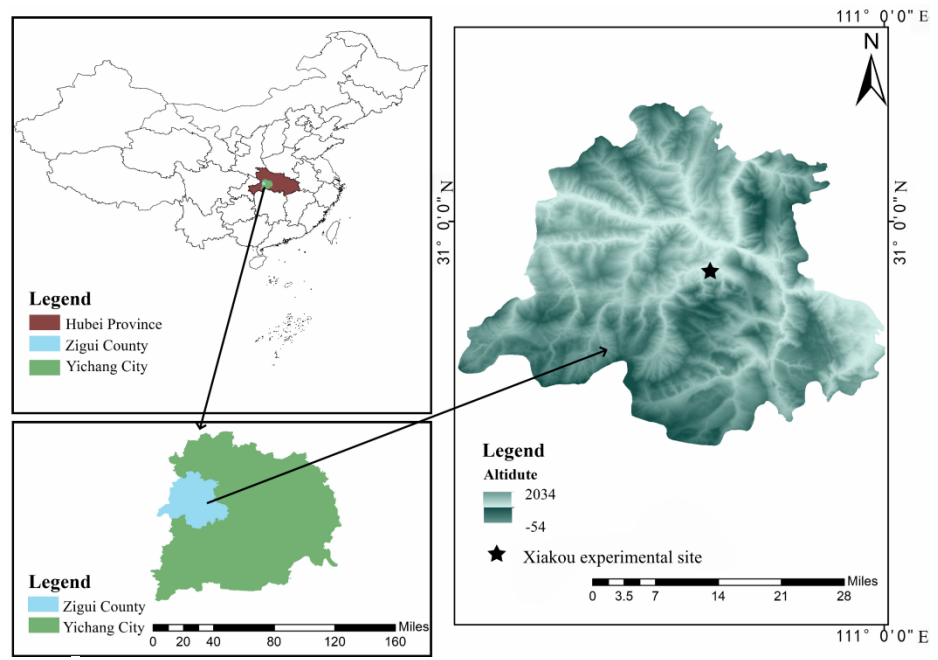


Fig. 1 Study Area Location

Based on the daily-scale measured rainfall and reservoir water-level data from 2023–2024, the correspondence between rainfall events and the dynamic response of the reservoir water level was analyzed. Undisturbed soil samples were collected from the water-level fluctuation zone (elevation 150–170 m) at the Xiakou experimental site in the Three Gorges Reservoir area. Shear strength parameters (cohesion, c, and internal friction angle, ϕ) were obtained through laboratory triaxial shear tests, and the saturated hydraulic conductivity (k_s) was determined from permeability tests. Subsequently, an unsaturated hydraulic model for the bare soil was established by combining these results with data from Soil-Water Characteristic Curve (SWCC) tests.

Building upon this, typical flood-tolerant plant species cultivated in-situ were selected. The tensile strength of their roots was measured via single-root tensile tests. Simultaneously, direct shear tests on root-soil composites were conducted to quantify the enhancement effect of the root system on soil cohesion and its hydraulic reinforcement role. To account for the influence of artificial drainage measures on the slope's hydraulic properties, the geometric layout of the drainage system was determined in the model based on field investigations. The system was parameterized by defining its core hydraulic components as high-permeability units to realistically simulate their function in rapidly dissipating pore water pressure.

III. Methodology

This study proposes a multivariate joint probability modeling framework for assessing the stability of bank slopes in the water-level fluctuation zone (WLFZ), an area subject to intense reservoir regulation (Figure 2). In this region, the periodic rise and fall of the water level accelerate the degradation of the rock and soil mass. The proposed framework is designed to be closely coupled with numerical simulation platforms such as GeoStudio and COMSOL. Based on measured rainfall and water-level data, the framework identifies the typical joint triggering conditions that induce bank slope deformation and landslides. It then constructs a joint distribution model capable of quantifying risk, enabling the prediction of slope failure probability under various coupled paths of rainfall intensity-duration and water-level change. Furthermore, the framework integrates the dual mechano-hydraulic reinforcement effects of vegetation, allowing for a quantitative evaluation of the influence of WLFZ protection plants on slope stability.

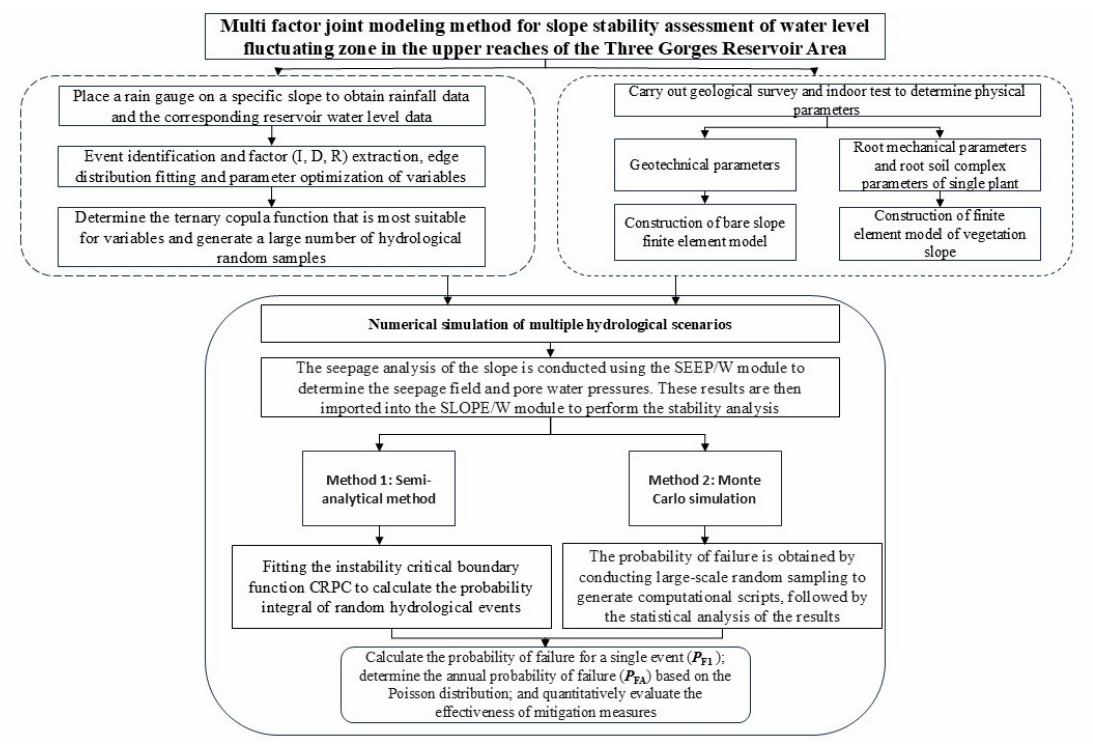


Fig. 2 The research framework

3.1 Joint Distribution Modeling of Hydrological Triggering Factors

3.1.1 Construction of Marginal Distributions

A precise quantification of the joint probability characteristics of rainfall and water-level variations is necessary for assessing the failure probability of bank slopes in the water-level fluctuation zone. In this study, rainfall I, D, and R are selected as the core hydrological disturbance variables. A trivariate joint distribution is established based on copula theory to characterize their joint occurrence frequency, thereby representing the failure risk mechanism under the synergistic action of multiple factors (Gariano et al. 2014). Each identified independent rainfall event is characterized by its I and D, and is then matched with the corresponding synchronous or lagged R to form the trivariate sample dataset I, D, R).

To evaluate the goodness-of-fit of different probability distributions for I and R data, four common candidate distributions were initially selected for a comparative analysis of marginal modeling. The fitting performance of each model was quantitatively assessed using the Akaike Information Criterion (AIC), the Bayesian Information Criterion (BIC), and the Kolmogorov-Smirnov (K-S) goodness-of-fit test statistic. The AIC and BIC are expressed as:

(1) (2)

where k is the number of model parameters, L is the maximum value of the likelihood function, and n is the sample size. Lower values for the AIC and the K-S test's D statistic, along with a p-value approaching 1, indicate a better fit for the marginal distribution.

Given that the daily-scale D is an inherently discrete variable, typically taking integer values between 1 and 6 days, its distribution exhibits distinctly non-continuous, asymmetric, and discrete characteristics. To more accurately reflect these sample features, this study employs a non-parametric Kernel Density Estimation (KDE) method to construct the marginal distribution of D. This approach generates a smooth, continuous probability density function by placing a kernel function at each data point and summing them.

3.1.2 Copula-Based Trivariate Joint Modeling

To quantify the joint distributional relationship among I, D, and R, this study introduces the copula function based on Sklar's theorem to establish a trivariate joint distribution model. According to Sklar's theorem, any multivariate joint distribution function can be decomposed into its constituent marginal distribution functions and a unique copula function that describes their dependence structure.

(3)

Where, is the trivariate joint distribution function of the variables I, D, and R, is the trivariate copula function, which describes the dependence structure among the three variables, are the marginal distribution functions for the variables I, D, and R, respectively.

$$C_R(u_1,u_2,...,u_d) = \Phi_R(\Phi^{-1}(u_1),\Phi^{-1}(u_2),...,\Phi^{-1}(u_d))$$

where, C_R denotes the joint cumulative distribution function (CDF) of the Gaussian copula. The function $\Phi^{-1}(u_d)$ is the inverse of the standard normal CDF (i.e., the quantile function), which transforms the marginal probabilities from the uniform domain to the Gaussian domain. Furthermore, Φ_R signifies the joint CDF of a d-dimensional standard normal distribution with a zero mean vector and a correlation matrix R. The matrix R serves as the parameter of the copula, defining the linear dependence structure among the variables. is the copula joint distribution function, are the values of the marginal distribution functions for the variables, is the single dependence parameter of the copula, which controls the strength of the association among the variables.

After constructing the trivariate joint copula distribution, a large number of pseudo-observations are generated using the marginal distribution functions. These samples are then inverse-transformed back into sets of the actual physical variables for use in the failure criterion analysis and numerical simulations.

Using the Monte Carlo method, a large set of pseudo-observation sample points, is generated by sampling from the copula function, with each dimension falling within the range. To transform these pseudo-observations from the uniform space back into the original physical space, the inverse of each marginal distribution function is used as follows:

Since the actual values of R in reality include both positive (drawdown) and negative (rise) values, the inverse-transformed R values are subsequently subjected to a centering shift. This adjustment allows the simulated R to more realistically reflect the actual hydrological conditions, yielding a set of slope boundary condition combinations that represent the simulated trivariate stochastic hydrological scenarios.

3.2 Generation of Stochastic Hydrological Scenarios Based on Regionalized Huff Curves

Slope stability is controlled not only by the total rainfall amount but is also significantly dependent on the rainfall intensity and its temporal distribution characteristics (Bordoni et al. 2020). The daily-scale stochastic hydrological events generated by the copula model have insufficient temporal resolution to directly drive the physical model, which requires high-resolution inputs. To bridge this scale gap and to accurately represent the key features of hazardous rainfall processes, this study introduces the regionalized Huff curve method to perform temporal downscaling on the daily rainfall data.

This method, through a non-dimensionalization process, classifies rainfall hyetographs into four typical storm patterns. This allows for the reproduction of the peak intensity and dynamic evolution of storm events, thereby ensuring the simulation accuracy of the pore water pressure response.

The parameters for the Huff curves were derived from the statistical analysis of long-term, high-resolution rainfall data from the Three Gorges Reservoir area (Zhang et al. 2021). Given the distinct regional characteristics of the rainfall patterns in this area and the need for differentiated downscaling strategies for events of different risk levels, this study classifies the simulated events into two categories based on the China Meteorological Administration's definition of a rainstorm (24-hour precipitation, $P \ge 50$ mm): rainstorm and non-rainstorm events.

For rainstorm events, the second-quartile (2nd Quartile), 50th-percentile Huff curve, which represents the typical hazardous storm pattern in the Three Gorges Reservoir area, is selected. This curve is used to non-uniformly distribute the total rainfall amount (P) over the event duration (D). For non-rainstorm events, their hydrological effect is considered to be primarily slow, antecedent soil water accumulation, thus avoiding the artificial introduction of unrealistic intensity peaks.

Ultimately, the stochastic hydrological events generated by the copula model are converted into hourly rainfall hyetographs. These hyetographs, in conjunction with the corresponding R, form the set of dynamic boundary conditions for the numerical simulation of slope stability. This process achieves the coupled modeling of hydrological stochasticity and the physical response of the slope.

3.3 Numerical Modeling of the Physical Slope Response

3.3.1 Finite Element Model Setup

Based on the typical binary sedimentary structure of the soil-mantled bank slopes in the upstream Three Gorges Reservoir area, which consists of an upper layer of silty clay overlying a lower bedrock stratum, this study developed a two-dimensional 2D finite element model under the assumption of isotropic and homogeneous material properties.

The model geometry was established according to the actual morphology of the bank slope, with a profile width of 470.0 m, a height of 246.0 m, and a slope angle of 22° (Figure 3). The model domain was

(5)

(4)

discretized into a hybrid mesh of triangular and quadrilateral elements (element size ≈ 3 m), comprising a total of 10,065 nodes and 9,863 elements. The physical and mechanical parameters of the soil, determined from laboratory tests (Table 1), were assigned to the corresponding elements to represent the material properties. The numerical simulation was conducted in three sequential stages: (1) The rate of water-level drawdown and the initial reservoir water level were determined in accordance with the operational regulations of the Three Gorges Reservoir. (2) A steady-state seepage analysis was first performed under the constant initial water level to simulate the initial moisture distribution within the saturated and unsaturated zones. (3) The rainfall event was then coupled with the water-level drawdown process, proceeding with a time step of 2 hours. In this stage, the modified Mohr-Coulomb failure criterion was employed to describe the shear strength degradation characteristic of the unsaturated soil, and the factor of safety (FS) was iteratively calculated using the Morgenstern-Price method.

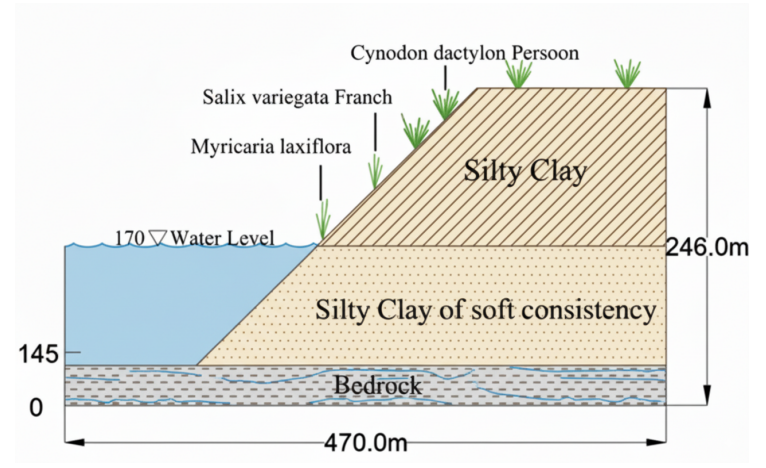


Fig. 3 Simplified slope profile model of the study area

Table 1 Parameters of rock and soil mass in the reservoir area

Hydraulic parameters	Shear strength parameters		
Saturated volumetric water	40	Saturated unit	20.1
content /%		weight/ $(kN \cdot m^{-3})$	
Residual volumetric water	4	Effective	13.6
content/%		cohesion/kpa	
Saturated hydraulic	5.11×10^{-6}	Effective friction	15.9
conductivity / (m/s)		angle/ (°)	

3.3.2 Quantification of the Protective Effects of Vegetation

To quantify the influence of vegetation on slope stability, this study developed a root-reinforcement effect model based on the typical slope-protection plants: *Cynodon dactylon Persoon*, *Salix variegata Franch*, and *Myricaria laxiflora*. The plants were configured in a shrub-grass gradient, planted at 2.0 m intervals on the slope surface to form a multi-layered protective structure.

Three comparative scenarios were established to analyze the soil reinforcement effects of vegetation and the synergistic enhancement mechanism of engineering measures: (1) a bare soil slope; (2) a vegetated slope; and (3) a combined vegetation-drainage protection system.

The mechanical reinforcement effect is primarily reflected by the tensile strength of roots. According to in-situ and laboratory tensile tests (Fig. 5), the tensile strength of different plant roots exhibits a significant negative power-law relationship with root diameter, and the root–soil composite can be approximately assumed to be horizontally uniform. Based on typical growth habits and root morphology classification (Fig. 4b), the root system of *Cynodon dactylon* is shallow-rooted and resembles a Exponential/Shallow architecture; *Salix variegata Franch* is a shrub species with a distribution approximating a Conical form; while *Myricaria laxiflora* shows a concentration of roots in the middle soil layer, corresponding to an Globular distribution. In the numerical model, plant roots are simplified using a soil-nail analogy, with mechanical parameters determined from the measured root diameter–tensile strength relationship and the above distribution patterns. The rooting depth of *C. dactylon* is set to 0.8–1.0 m, while that of *M. laxiflora* and *S. variegata* is set to 1.5–2.5 m. Compared with the reinforcing effect, the self-weight of roots has a negligible influence on slope stability and is therefore omitted in the calculations for simplification.

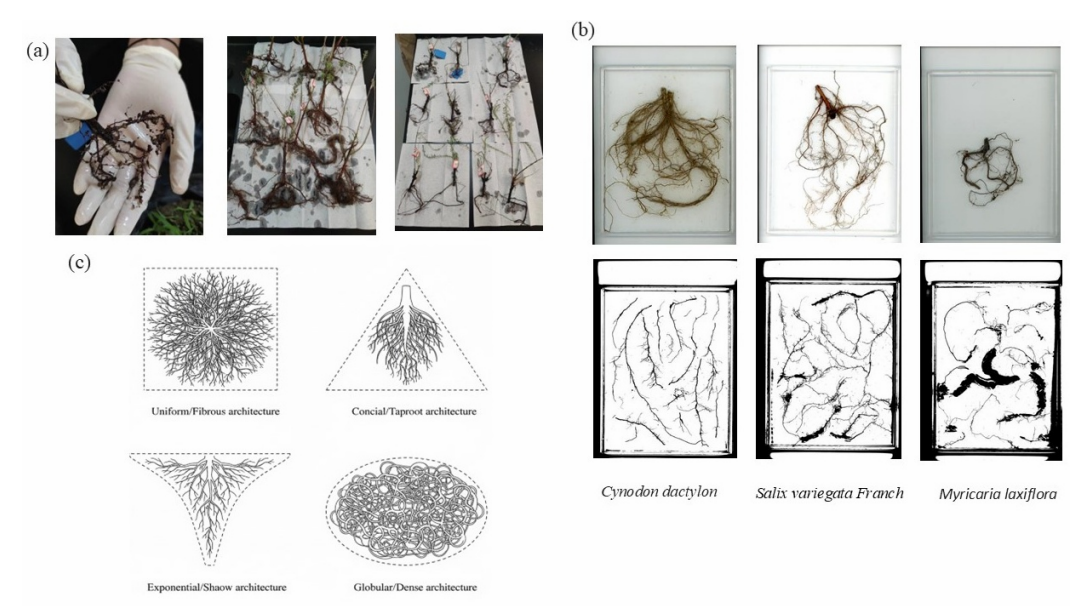


Fig. 4 a Handling of plant roots. b Complete Root System Diagram and Scanned Image. c Different plant root architectures

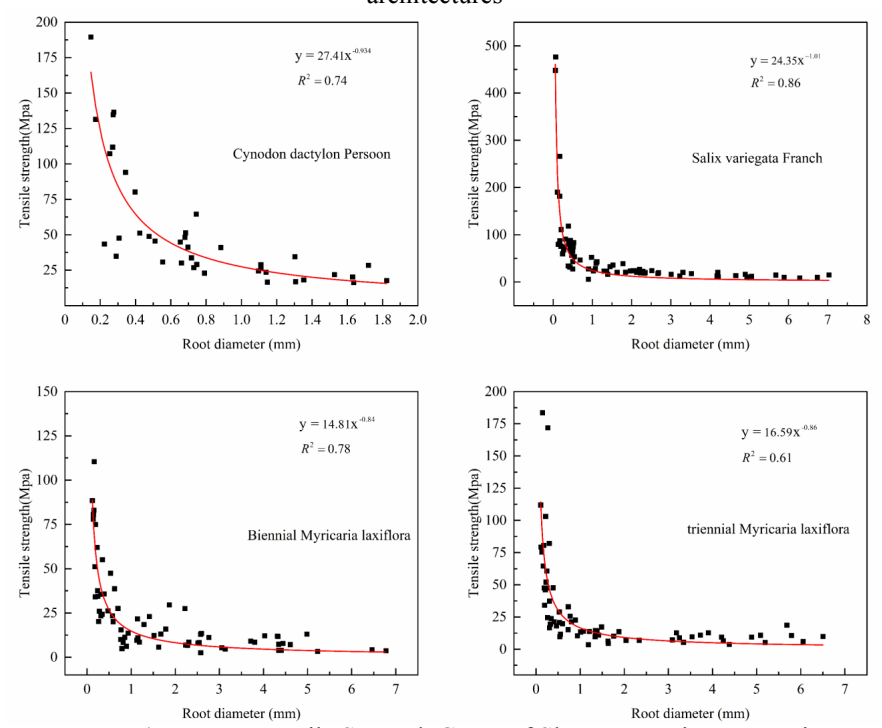


Fig. 5 Root Tensile Strength Curve of Slope Protection Vegetation

The hydraulic effect of vegetation is primarily manifested as a root-induced alteration of the soil's hydraulic conductivity. Based on the hydrological response mechanism where plant root systems create preferential flow paths, this study set the saturated hydraulic conductivity of the root-soil composite to be four times that of the bare soil. This assumption is consistent with the established principle that vegetation roots enhance the hydraulic conductivity by increasing the volume of non-capillary macropores. The shear strength parameters were determined from laboratory direct shear tests; the relevant mechanical and hydraulic parameters are presented in Table 2.

Table 2 Parameters of root-soil composite

Hydraulic parameters		Shear strength parameters			
Saturated volumetric	water	44.3	Saturated	unit	21.4
content /%		weight/	$(kN \cdot m^{-3})$		
Residual volumetric	water	8	Effective cohes	ion/kpa	23.5
content/%					

Saturated hydraulic 2×10^{-5} Effective friction 25 conductivity / (m/s) angle/ (°)

3.3.3 Setup of Scenarios for Water-Level Fluctuation Response Analysis

To investigate the evolutionary behavior of slope stability under the isolated effect of reservoir water-level fluctuations and to identify the primary failure risk scenarios, this study conducted a response analysis of two distinct slope models subjected to water-level changes without the interference of rainfall.

By imposing three typical water-level drawdown rates 0.3 m/day, 0.6 m/day, and 1.2 m/day the differential effects of the rising and falling water-level processes on the slope's factor of safety were compared. This analysis provides a foundational basis for selecting the dominant failure-inducing scenarios for the subsequent construction of the Critical Rainfall Pattern Curve (CRPC), with the aim of elucidating the differentiated impacts of various water-level fluctuation rates on slope stability.

3.4 Critical Rainfall Triggering Boundary Function

To quantitatively characterize the triggering mechanism of slope failure under the coupled effects of rainfall and water-level fluctuation, this study develops a three-dimensional (3D) CRPC based on the results of coupled seepage-stress numerical simulations. This function is defined as a parametric surface in the space of triggering variables that corresponds to the critical state of the factor of safety (FS = 1.0), and it is used to identify the critical failure conditions for combinations of I, D, and R.

The data points for the CRPC are obtained using a hybrid strategy that combines the control variate method and the bisection method. First, a specific (I,R) combination is selected within a predefined parameter range. The rainfall duration (D) is then sequentially adjusted, and the finite element analysis is run iteratively until the critical condition $(FS \approx 1.0)$ is met. To enhance the search efficiency, the bisection method is employed to ensure that the error in the factor of safety converges to a preset tolerance (|FS - 1.0| < 0.01). The resulting critical rainfall duration is denoted as Dc. By iterating through multiple (I,R) combinations, a set of discrete sample points representing the critical state is generated, which constitutes the discrete CRPC dataset.

Based on this discrete dataset, a non-linear regression method is introduced to establish a continuous predictive model. A power-law empirical function is selected, grounded in the physical principles governing rainfall and water-level threshold mechanisms:

where the coefficients b and c are the sensitivity indices of the slope stability with respect to rainfall intensity and the rate of water-level drawdown, respectively; d represents the baseline stability offset of the slope; and a is the regression coefficient.

3.5 Failure Probability Assessment Based on Joint Scenarios

The construction of the CRPC provides an efficient semi-analytical pathway for estimating the single-event failure probability (P_{F1}). The core of this method involves integrating the joint probability density function of the hydrological triggering factors over the failure domain defined by the CRPC surface. Given the method's dependence on the fitting accuracy of the CRPC function, this study introduces a Monte Carlo Simulation (MCS) framework as a complementary approach, aimed at establishing a benchmark for the direct, physics-based calculation of failure probability. A large ensemble of random scenarios is generated by the copula-based hydrological joint model and then coupled with a physical stability model to ultimately derive the annual bank slope failure probability (P_{FA}).

The analysis procedure is initiated by generating N independent hydrological scenarios, each defined by key characteristic variables: peak rainfall intensity, rainfall duration, and the rate of water-level change. For each individual scenario j, the daily-scale rainfall parameters are first disaggregated into a high-resolution hourly rainfall hyetograph $I_j(t)$, using a conditional downscaling method informed by the event storm type. This hyetograph, along with its corresponding water-level boundary $R_j(t)$, is then used as dynamic boundary input for a finite element model. Subsequently, a coupled, transient unsaturated seepage-stability analysis is executed to obtain the time-history curve of the factor of safety for that scenario. The minimum value from this curve is extracted as the critical failure criterion. This entire process is repeated for all N scenarios, and the resulting collection of outcomes is used to statistically quantify the annual failure probability and evaluate the effectiveness of vegetation protection.

Probabilistic Quantification: Based on the collected set of FS min results from all scenarios, the number of failure events is counted according to the failure standard of FS < 1.0. The failure probability (P_{F1}) is then calculated by the following equation (Aleotti and Chowdhury 1999):

(6)

(7)

Annual Probability Derivation: To account for the stochastic nature of the number of hydrological events within a year, the annual number of events, N, is assumed to follow a Poisson distribution with a rate parameter λ . Based on the law of total probability, P_{FA} is then expressed as (Huang et al. 2018):

(8)

Lifetime Probability Derivation: To assess the long-term risk over the entire design life of the slope, the cumulative failure probability over an M-year design life (P_{FM}) is introduced. Assuming that failure events in different years are statistically independent, P_{FM} can be derived from the P_{FA} using the following relationship:

(9)

IV. Results

4.1 Statistical Characteristics and Correlation of Hydrological Triggering Factors

Based on the measured data from 2023–2024, the statistical properties of the key hydrological triggering factors and their coupled relationships were analyzed to identify potential multi-factor interaction patterns and to provide a basis for the subsequent joint probability modeling.

The frequency distribution of the water-level fluctuation magnitude (ΔH), shown in Figure 6, reveals that for approximately 64% of the rainfall events, ΔH was less than ± 1.0 m. The distribution is right-skewed, indicating that while most events were associated with minor water-level changes, extreme responses involving drawdowns exceeding 2.5 m also occurred. The skewness and slight bimodal structure of this distribution suggest that the reservoir's response to rainfall deviates from a classic normal distribution, reflecting the non-linear coupled characteristics of the regulation mechanism and the magnitude of rainfall.

The time-series plot of rainfall events superimposed on the water-level hydrograph shows that intense rainfall events were concentrated during the reservoir drawdown phases. Typical examples of this occurred in mid-September 2023 and early June 2024, indicating a high joint probability of occurrence for rainfall and water-level drawdown, which highlights the hazard risk from this "synergistic triggering" effect. An analysis of ΔH over the 48-hour period surrounding each rainfall event found that 41% of events were accompanied by a significant water-level drop ($\Delta H < -0.5$ m), whereas only 25% were associated with a significant rise ($\Delta H > 0.5$ m). This finding demonstrates that the reservoir's response to rainfall is neither linear nor symmetric. A simple causal chain of "rainfall leads to water-level rise" does not exist; instead, the response is governed by complex, non-linear behavior dominated by reservoir operation.

In summary, the rainfall and water-level fluctuations exhibit asymmetric, non-independent, and temporally correlated behavior. These characteristics constitute a significant statistical coupling, a finding that provides the theoretical and data foundation for constructing a multivariate joint probability model for hazard assessment.

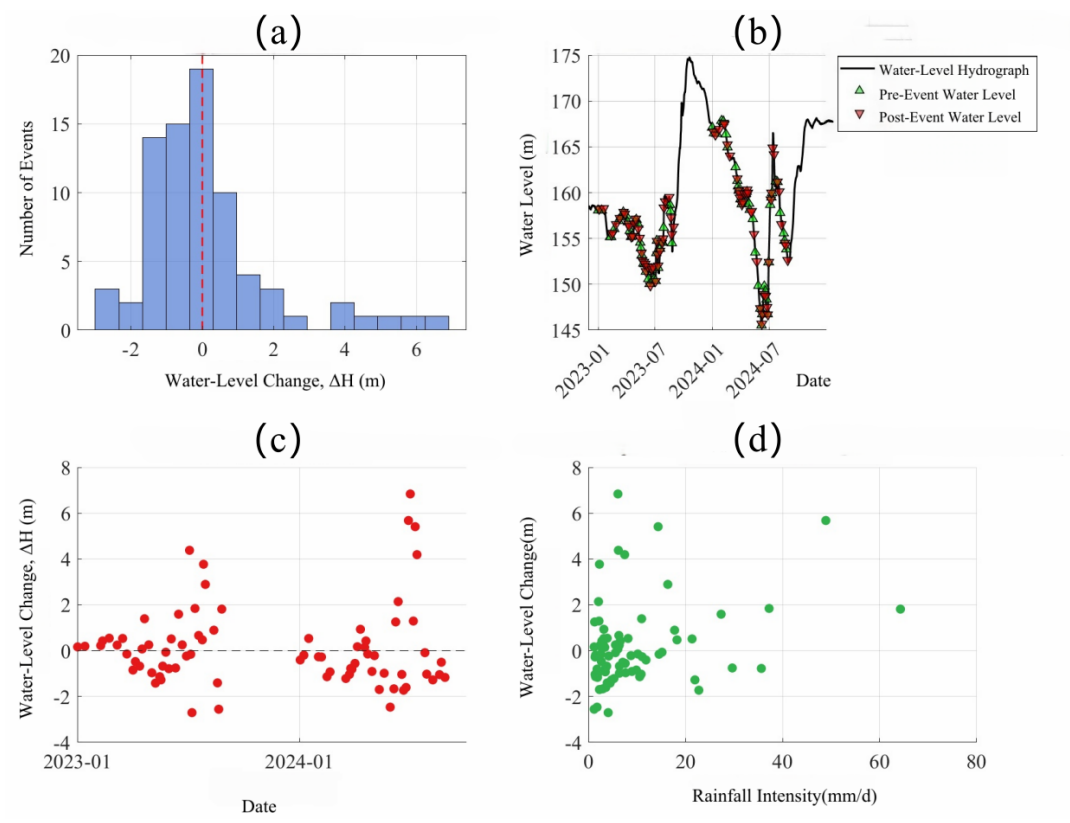


Fig. 6 Statistical Characteristics of Hydrological Triggering Factors. **a** Frequency Distribution of Water-Level Change. **b** Water-Level Hydrograph with Superimposed Rainfall Events. **c** Water-Level Change per Rainfall Event. **d** Relationship between Water-Level Change and Mean Rainfall Intensity

To construct the joint distribution model, the marginal distribution for each random variable (I, D, R) must first be determined. Following an evaluation of multiple candidate probability distribution functions (Table 3), the Lognormal distribution was found to provide the best fit for I, while the Gamma distribution was most suitable for fitting R. For the discrete variable D, a non-parametric Kernel Density Estimation (KDE) was employed to construct its marginal distribution. The selected marginal distributions and their corresponding fitted parameters are summarized in Table 4.

Table 3 Comparison of Fitted Parameters and Goodness-of-Fit from Candidate Distributions for

Variable				
Variable	Fitted	AIC	BIC	Log-likelihood
Dis	tribution			
Intensity (I)	Lognormal	246.6	250.1	-120.3
	GEV	251.4	254.9	-122.7
	Gamma	252.8	256.0	-123.4
	Exponential	284.4	286.7	-140.2
Rate (R)	Gamma	203.0	207.4	-98.5
	Lognormal	204.0	208.5	-99.0
	GEV	218.6	223.0	-101.2
	Exponential	233.6	236.0	-115.8

Table 4 Fitted Parameters of Marginal Distributions for Rainfall Intensity, Duration, and Water Level Fluctuation Rate

Variable	Fitted Distribution	Distribution Parameters
Intensity (I)	Lognormal	$\sigma = 0.5, \theta = 20.1, \mu = 1.67$
Duration (D)	Kernel Density Estimation (KDE)	Bandwidth=0.4
Rate (R)	Gamma	$\alpha = 2.85, \beta = 1.25$

A trivariate Gaussian Copula joint distribution was constructed using pseudo-observations derived from the inverse of the optimal marginal distributions. Figure 7 displays a three-dimensional scatter plot of 1,000 samples simulated by this model within the standardized unit hypercube.

www.ajer.org

The results reveal that the samples are highly concentrated and exhibit strong linear covariation in the I and D dimensions. A Kendall's τ coefficient of approximately 0.98 for I and D confirms an extremely strong dependence, indicating that rainfall intensity and duration co-vary synergistically in the Three Gorges Reservoir area. Conversely, samples in the R dimension are moderately dispersed. This reflects a degree of synchronicity between water-level fluctuations and rainfall events, yet also a considerable uncertainty attributable to the influences of reservoir operations and inflow processes. Overall, the model effectively captures the holistic dependence structure of the hydrological factors.

Spatially, the clustering of samples in the lower-value (left-tail) region indicates a high probability of joint occurrences of low-to-moderate intensity, short-duration rainfall events with moderate-to-high water-level drawdown rates; such scenarios are prone to triggering bank slope instability in the reservoir area. In contrast, the sparse distribution of samples in the upper-value (right-tail) region suggests a low joint probability for extreme rainfall and rapid drawdown events. However, their potential impact on slope failure cannot be overlooked. Subsequent analysis must therefore integrate a critical failure boundary function to quantify the distinct contributions of these different tail regions, thereby unifying the statistical model with the physical failure mechanisms.

Table 5 Kendall's Tau () Correlation Matrix for Rainfall Intensity (*I*), Duration (*D*), and Water Level Fluctuation Rate (*R*)

1 idetation rate (n)			
•	Intensity (I)	Duration (D)	Rate (R)
Intensity (I)	1.00	0.98	0.52
Duration (D)	0.98	1.00	0.41
Rate (R)	0.52	0.41	1.00

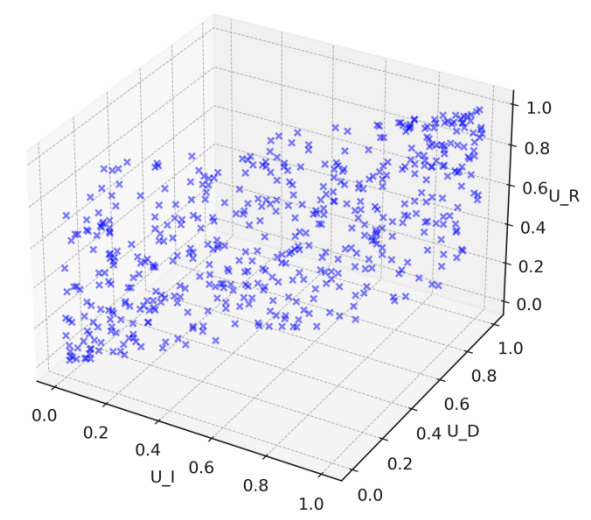


Fig. 7 Three-dimensional scatter plot of samples simulated by the trivariate Gaussian Copula model 4.2 Response of Slope Stability to Water-Level Fluctuations

Based on the time-history evolution of the factor of safety (FS) for the reservoir bank slope, as presented in Figure 8, it is evident that the dynamic stability response is significantly influenced by the combined effects of rapid water-level drawdown and vegetation cover.

Regardless of the presence of vegetation, an increase in the drawdown rate (R) accelerates the decline of the FS. Under bare slope conditions, when R = 1.2 m/d, the FS only requires approximately 6 days to drop to its critical value, whereas for R = 0.6 m/day, the FS remains consistently above 1.05. Vegetation protection results in an overall upward shift of the FS curves. Taking R = 0.3 m/d as an example, the minimum FS of the bare slope is 0.97, while the vegetated slope maintains an FS of around 1.2, which is significantly above the failure threshold. The average increase in stability across the different R values ranges from approximately 12% to 24%, confirming the root system's soil reinforcement and anti-sliding capacity during drawdown periods.

Conversely, the process of a rising water level exhibits a dual effect on stability. Although seepage increases pore water pressure, the buttressing effect of the reservoir water at the slope toe and the confining hydrostatic pressure are the dominant factors in most scenarios. As shown in Figure 8(b), the FS of the bare slope generally increases by 6%–10% during the water-level rise period, with its peak value at times even surpassing that of the vegetated slope.

Given that the drawdown process represents the primary failure-inducing scenario in the reservoir area, this study uniformly defines R as a positive value (representing the drawdown rate) when constructing the CRPC. This is done to emphasize the dominant role of the coupled "rainfall-drawdown" mechanism in triggering landslides in the region.

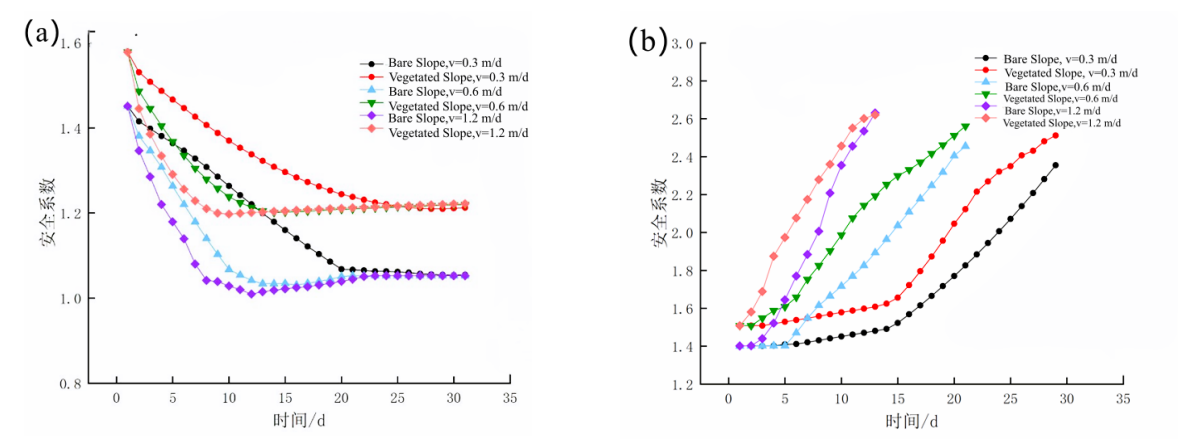


Fig. 8 (a) Variation of Factor of Safety during water-level drawdown.; (b) Variation of Factor of Safety during water-level rise

4.3 Critical Rainfall-Drawdown Pattern Curves under Different Scenarios

Figure 9 reveals the multivariate coupled relationship among D_c , I, and R. The response surface shows that D_c exhibits a hyperbolic decreasing trend with increasing I and R, indicating that the combined effect of intense rainfall and rapid water-level drawdown significantly shortens the critical time to slope failure.

Within the range of $5 \le I \le 100$ mm/h and $0.3 \le R \le 4$ m/day, D_c can be characterized by a power-law function ($R^2 = 0.966$), where the negative exponents for I and R are -0.450 and -0.605, respectively. This quantitatively confirms their negative correlation with the critical duration. The absolute value of the exponent for R (0.605) is greater than that for I (0.450), demonstrating that the stability of the bare soil slope is more sensitive to the rate of water-level drawdown than to rainfall intensity.

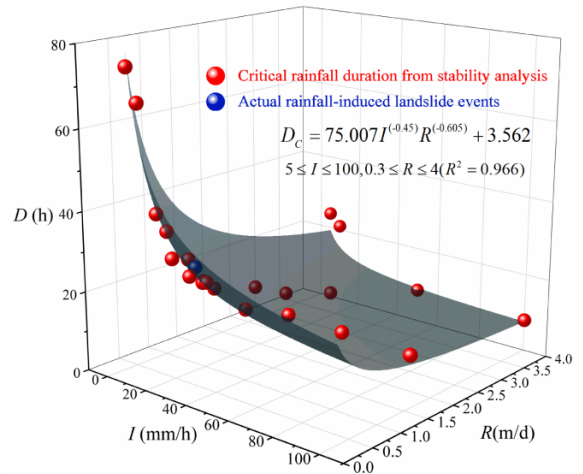


Fig. 9 The CRPC surface for the bare slope under the combined effect of rainfall and water-level drawdown

To evaluate the engineering protection measures, the CRPC surfaces for two typical protected slope scenarios were constructed, as shown in Figure 10. Compared to the bare slope, the presence of vegetation causes an overall upward shift of the CRPC surface, with the constant term increasing from 3.562 to 12.529. However, the sensitivity exponent for I(-1.322) is far greater in magnitude than that of the bare slope (-0.45), indicating that under intense rainfall, root-induced preferential flow accelerates infiltration and exacerbates the buildup of pore water pressure at depth, leading to a sharp deterioration in stability.

After the installation of a drainage system, the constant term of the CRPC surface is further elevated to 23.531, while the sensitivity exponents for I and R are reduced (-0.984 and -0.918, respectively). This demonstrates that the drainage system effectively dissipates pore water pressure, thereby attenuating the triggering effect of the hydrological boundaries on the failure probability.

The sensitivity analysis reveals a "retrogressive evolution" risk associated with the protective measures under specific coupled conditions. In a combined scenario of "extreme rainfall + medium water level," the

minimum $D_{\rm C}$ of the vegetated slope drops to 13 hours, which is paradoxically 7.1% lower than that of the bare slope. This confirms that root-induced preferential flow can create structurally weak zones. Furthermore, when the drainage system intersects the potential slip surface, a localized "secondary depression" appears on the CRPC surface. The critical I in this case is 1.2-5.5 mm/h lower than in the non-drained scenario, suggesting that under extreme rainfall, the drainage system may intensify groundwater convergence, inducing a rapid increase in pore pressure. These results indicate that neglecting the coupled hydro-mechanical effects could lead to a design paradox where "local optimization triggers global failure.

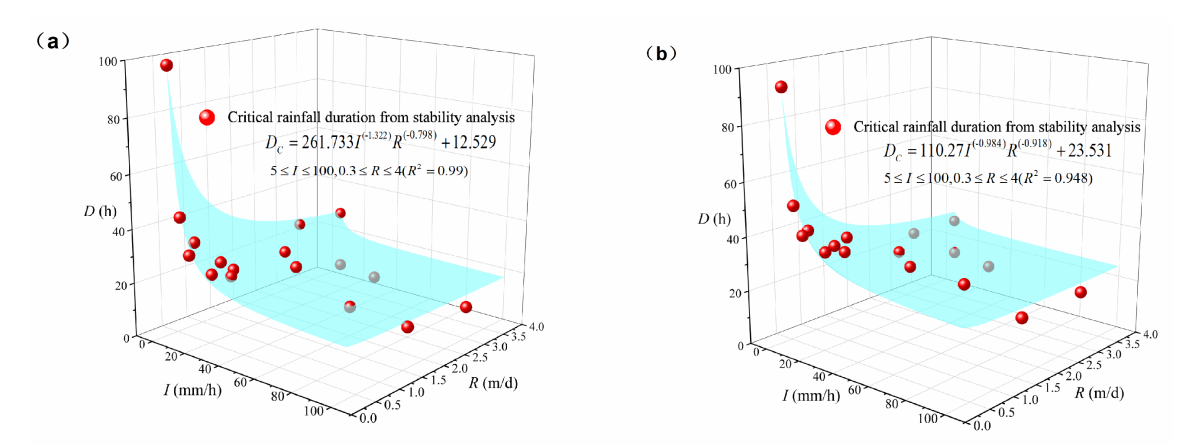


Fig. 10 The CRPC Surface for the Vegetated Slope under the Combined Effect of Rainfall and Water-Level Drawdown. **a** Slope without drainage measures. **b** Slope with drainage measures

4.4 Assessment of Slope Failure Probability

Based on the proposed probabilistic-physical coupled framework, a Monte Carlo simulation of 1000 stochastic hydrological scenarios was conducted to quantitatively assess the bank slope failure risk and the effectiveness of different eco-protection measures. Based on two years of measured data, the mean annual frequency of independent hydrological events (λ) was determined to be 24. Table 6 summarizes the failure probability assessment results for the three slope scenarios.

The analysis reveals that under the coupled effects of natural rainfall and water-level fluctuations, the bare slope in the water-level fluctuation zone exhibits a single-event P_{FI} of 5.6%, which translates to a high P_{FA} of 73.9%. This result underscores the significant cumulative risk posed by high-frequency, moderate-intensity disturbances, confirming that the instability mechanism of bank slopes in the Three Gorges Reservoir area is not solely governed by singular extreme events but is also substantially driven by the cumulative effect of frequent disturbances.

With the introduction of a vegetated slope (without drainage), the single-event failure probability was nearly halved to 2.8%. Its annual survival probability was enhanced by a factor of 1.96 relative to the bare slope, quantifying the value of the mechano-hydraulic reinforcement from the root system in mitigating long-term risk. However, the annual failure probability remained at a substantial level of 48.9%, indicating that the protective capacity of vegetation alone is limited. This conclusion is further corroborated by the CRPC surface analysis, which suggests that under intense rainfall, root-induced preferential flow could become a potential risk factor in the absence of effective drainage.

A qualitative improvement in protection was achieved when vegetation was combined with a properly designed drainage system. The single-event failure probability was further reduced to 1.6%, and the annual survival probability increased to 68.1%, corresponding to a Protective Effectiveness Factor of 2.61 compared to the bare slope. This demonstrates that the drainage system effectively dissipates the pore water pressure generated by surface infiltration and preferential flow, creating a highly efficient synergy with the mechanical reinforcement from vegetation. This combined approach significantly enhances the slope's resilience to complex hydrological loads.

Table 6 Evaluation of Failure Probability and Effectiveness of Protective Measures under Various Bank Slope Scenarios

	L	stope seemand	13	
Slope Scenario	D	D	Annual	Survival Effectiveness of
	P_{F1}	P _{FA} Probability	Protection	
Bare Slope	5.6%	73.9%	26.1%	1
Vegetated Slope without Drainage	2.8%	48.9%	51.1%	1.96
Vegetated Slope with Drainage	1.6%	31.9%	68.1%	2.61

4.5 Long-Term Risk Evolution of Bank Slopes: From Annual Probability to Full Life-Cycle Assessment

Figure 10 reveals the sensitivity of the P_{FA} to the frequency of hydrological events(λ). The P_{FA} increases non-linearly with λ , underscoring the cumulative effect of high-frequency disturbances on risk. The efficacy of different protective measures in reducing annual risk is quantified by the vertical gap between the curves. As λ increases to a certain threshold, the annual risk approaches saturation, and the contribution of individual events diminishes. This indicates that in areas with high event frequencies, the absolute benefit of protective measures (i.e. the vertical gap between the curves) is most pronounced. The figure further illustrates the relationship between P_{FA} and the life-cycle failure probability (P_{FM}), providing a visual comparison of the long-term risk evolution pathways under the three protection scenarios. The red markers indicate the risk status at typical service lifespans, revealing the following key patterns:

Rapid risk amplification due to cumulative effects over the service life. As the service life (M) extends, the P_{FM} curves for all scenarios rapidly deviate from the 1:1 reference line, indicating significant long-term risk amplification. This effect is particularly pronounced in high-risk scenarios: for the bare slope, with a P_{FA} as high as 73.9%, the cumulative failure probability reaches 99.8% within just five years. In contrast, the risk saturation points for the vegetation-no drainage (P_{FA} =48.9%) and vegetation-with drainage (P_{FA} =31.9%) scenarios are reached at approximately 10 and 25 years, respectively. This suggests that if P_{FA} exceeds 30%, the cumulative risk will approach 100% within a relatively short service life.

The core value of protective measures lies in delaying the onset of risk saturation. The bare slope approaches risk saturation within five years, whereas the "vegetation + drainage" scenario postpones this point by approximately 25 years. This demonstrates that reducing the initial P_{FA} is crucial for delaying the attainment of the critical risk threshold. For high-risk bank slopes, merely extending the design life or increasing the factor of safety reserve is ineffective for risk mitigation. The fundamental solution is to proactively reduce the P_{FA} , thereby postponing cumulative risk saturation and ensuring the long-term safety and reliability of the engineering structure.

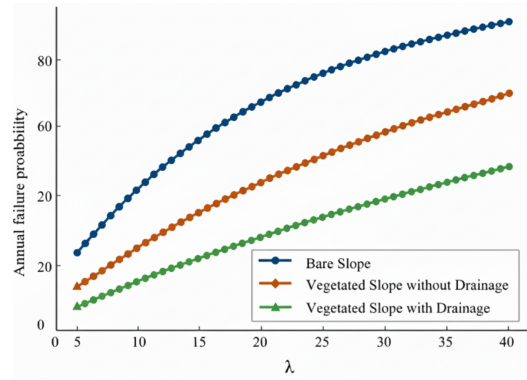


Fig. 10 Annual Failure Probability (P_{EA}) as a function of λ for different slope models

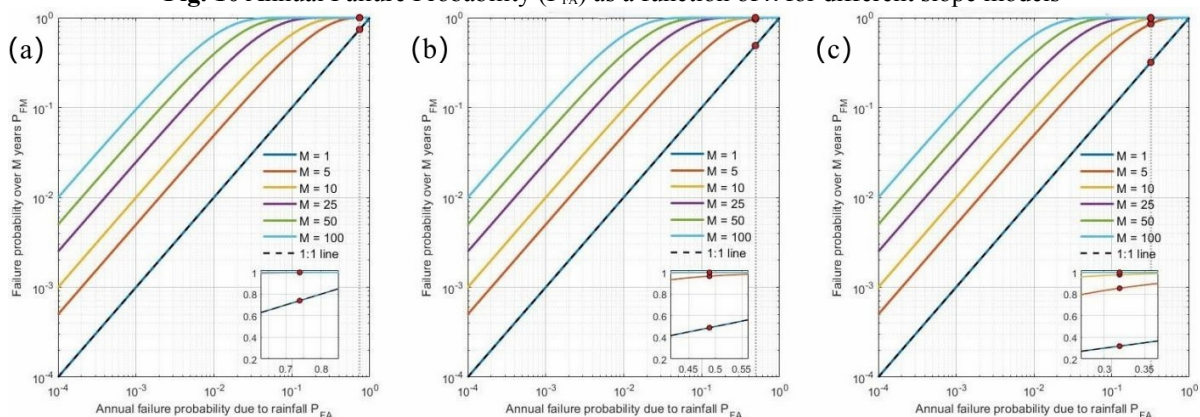


Fig. 11 P_{FA} as a function of λ for different slope models. a Bare Slope. b Vegetated Slope without Drainage. c Vegetated Slope with Drainage

V. Discussions

5.1 Non-linear Characteristics of Hydro-Factor Coupling and Risk Amplification

This study reveals the non-linear dependence structure among I, D, and R through a trivariate copula model. The Gaussian copula model exhibits significant lower tail dependence, indicating a high joint probability of occurrence for moderate-intensity rainfall events and rapid water-level drawdowns. This finding marks a

departure from the simplified assumptions of variable independence (Demisa et al. 2025) or linear correlation (Liu and Wang 2023) made in traditional research. By introducing *R* as a third dimension, the complex hydromechanical coupling mechanism driven by the dual forcing of "natural rainfall and anthropogenic regulation" in the Three Gorges Reservoir area is more realistically simulated. These results are consistent with the observational phenomena from typical landslide cases in the TGR reported by Zhao et al. (2017) and Hou et al. (2022), but this study, for the first time, provides a probabilistic quantification of this synergistic mechanism based on trivariate copula theory.

The CRPC analysis further demonstrates that *R* plays a dominant role in the failure process. This conclusion aligns with the simulation results of Jian et al. (2014) for a TGR landslide and the field observations of Huang et al. (2018) for the landslide. It shows that rapid water-level drawdown, by reducing the effective stress and matric suction of the soil, becomes a more efficient "preparatory disaster-inducing factor" than rainfall infiltration. The physical mechanism is twofold: a sudden water-level drop not only induces excess pore water pressure directed outward from the slope, weakening the shear strength (Springman et al. 2003), but also causes desiccation cracks in the WLFZ soil due to rapid water loss. These cracks provide preferential pathways for subsequent rainfall infiltration (Zhang et al. 2018), forming an amplified "drawdown-first, rainfall-second" hazardous sequence.

The non-linear amplification of failure probability also warrants attention. The annual failure probability is sharply amplified under the high-frequency hydrological disturbances of $\lambda \approx 24$. This annual risk is further amplified over the engineering design life, with the rapid saturation of the P_{FM} to a state of near-certainty. This underscores that even a moderate annual risk can translate into an unacceptable long-term hazard, a point often overlooked in conventional stability assessments. This finding is consistent with the view proposed by Gariano and Guzzetti (2016) in the context of climate change that "high-frequency, moderate-magnitude events may dominate long-term risk." Traditional landslide risk assessment methods based on extreme value theory focus only on the return period of singular extreme events (Guzzetti et al. 2008). In contrast, the cumulative risk assessment method proposed in this study, which is based on the full sequence of events, is more applicable to regions like the Three Gorges Reservoir area that are frequently affected by non-extreme disturbances.

5.2 Quantified Benefits and "Retrogressive Evolution" of Vegetation Protection

This study parameterizes the protective effects of vegetation; root reinforcement can increase cohesion to 23.5 kPa and the friction angle to 25°, which is consistent with the results of both laboratory and in-situ tests (Stokes et al. 2009). Through intertwining, anchoring, and consolidation effects, the root system significantly increases the apparent cohesion and internal friction angle of the soil (Waldron 1977; Norris et al. 2008), forming the core of the mechanical benefits of vegetation protection. This improvement in parameters causes an overall upward shift of the CRPC surface, significantly expanding the stable domain of the slope.

However, under a combined "intense rainfall + medium water level" scenario, the CRPC surface shows that the D of the vegetated slope is paradoxically lower than that of the bare slope. This phenomenon reveals the negative effect of the root-induced preferential flow mechanism. In intense rainfall scenarios, decomposed roots or the interfaces between roots and soil can form preferential pathways (Ghestem et al. 2011), allowing water to bypass the shallow soil layer with high matric suction and rapidly accumulate near the deep-seated potential slip surface (Bordoni et al. 2020). This process, defined in forest hydrology as "stemflow-induced infiltration" and "root-channel flow" (Johnson and Lehmann 2006), leads to the direct and efficient transport of water to deep, weak potential failure surfaces, threatening the overall stability of the slope (Liang et al. 2010). This study, for the first time in the context of the TGR's WLFZ, quantifies this "retrogressive evolution" risk through numerical simulation, highlighting the necessity of a systematic design for eco-protection.

Improper design of a drainage system can similarly induce failure risk. Under extreme conditions, the introduction of a drainage system results in a slight decrease in the D_c on the CRPC surface. If drainage pipes intersect a potential slip surface or if their outlets are poorly located, the system can transform into a "fast channel" for surface water to enter structural discontinuities or weak interlayers during extreme rainfall. This "pipe effect" can cause a rapid rise in pore water pressure at critical locations, with a hazardous efficiency that may even exceed that of diffuse infiltration in a non-drained scenario (Hutchinson 1977). Case studies of engineering failures have shown that the blockage of drainage holes or the diversion of water to unintended vulnerable areas are significant causes of slope failure (Take and Beddoe 2014). Therefore, the design of a drainage system requires careful consideration of the geological structure, the spatial relationship with potential slip surfaces, and the hydraulic pathways to avoid local optimization triggering a systemic failure.

5.3 Synergistic Benefits of Engineering and Ecological Measures

This study confirms that the synergistic configuration of vegetation and a drainage system is the optimal strategy for responding to complex hydrological disturbances. This conclusion not only numerically validates the theory of Griffiths and Fenton (2004)—that soil improvement can significantly enhance slope

reliability—but also extends the theoretical scope from the improvement of a single geotechnical parameter to the complex, multi-field coupling of vegetation, hydraulics, and engineering drainage.

The drainage system plays a key regulatory role in this synergy. By interrupting the risk chain of "intense rainfall \rightarrow preferential flow \rightarrow pore pressure accumulation \rightarrow failure," it allows the positive mechanical reinforcement benefits of vegetation to be fully realized (Coppin and Richards 1990) while simultaneously suppressing its negative hydraulic effect of enhanced infiltration (Ilstedt et al. 2007). This synergy transforms the protective effect from a linear addition to a non-linear multiplication, achieving an exponential increase in system stability. Ecological engineering practice has shown that single ecological measures often fail to achieve their intended goals due to their limited effects or potential risks, whereas the compatible integration of vegetation and drainage engineering can produce significant synergistic gains (Mickovski et al. 2009; Stokes et al. 2008). This result proves that eco-protection systems must follow principles of systematic design, using multi-element synergy to avoid the risk of global failure caused by local optimization.

5.4 Limitations and Future Prospects

The probabilistic model developed in this study is predicated upon a two-year hydrological dataset. The length of this time series presents inherent limitations in its capacity to capture long-term climatic variability and rare, extreme events. Consequently, the model exhibits considerable uncertainty for very long-term risk forecasting. The results should therefore be interpreted as a "scenario analysis" based on current hydro-climatic conditions, rather than a deterministic forecast of the future. With the continuous accumulation of monitoring data, the framework proposed herein can be progressively validated, calibrated, and optimized to enhance its long-term predictive reliability.

In the current study, soil parameters were treated as deterministic values. Future work could extend the model by incorporating the spatial variability of soil parameters, thereby establishing a "fully probabilistic" risk assessment framework that couples hydrological stochasticity with the randomness of geotechnical parameters. Furthermore, integrating such a point-scale, high-resolution model with regional-scale landslide susceptibility assessments holds the potential to bridge the gap between the risk assessment of individual bank slopes and the implementation of regional disaster early warning systems.

VI. Conclusions

This study develops and applies an integrated analytical framework, fusing probabilistic models with physical processes, to systematically quantify the instability mechanisms and risk evolution of bank slopes in the Three Gorges Reservoir's water-level fluctuation zone (WLFZ) driven by the combined effects of natural rainfall and reservoir operations.

A key finding reveals that slope instability is predominantly driven by the cumulative effects of high-frequency, moderate-intensity disturbances, rather than by rare, extreme events as is conventionally assumed. Under the impact of an annual average of 24 hydrological events, the P_{FA} for bare soil slopes reached 73.9%, clearly indicating that frequent rainfall-drawdown cycles are the primary driver of progressive structural degradation. Furthermore, this study pioneers the use of a trivariate Copula model to probabilistically characterize the strong non-linear and synergistic evolution among hydrological triggers. The model not only confirms a strong positive correlation between I and D during major rainfall events (Kendall's $\tau \approx 0.98$) but, more critically, captures the high joint occurrence probability of moderate-to-low intensity rainfall and moderate-to-high drawdown rates. A Conditional Reliability and Probability of Combination (CRPC) analysis further quantifies that slope stability is 1.7 times more sensitive to the R than to rainfall I. Together, these findings uncover the latent disaster-inducing potential of non-extreme combined scenarios, such as "gentle rainfall-rapid drawdown."

To address this complex risk mechanism, the research validates the decisive role of synergistic ecological-engineering measures in ensuring long-term safety. A combined "vegetation-drainage" configuration drastically reduces the P_{FA} to 31.9%, achieving a protection benefit factor of 2.61, an effect far superior to any single measure. This proactive reduction of annual risk is crucial, as a full life-cycle risk analysis shows that once the P_{FA} exceeds 30%, P_{FM} rapidly saturates towards certainty within a typical engineering design life.

This framework provides a robust quantitative tool for dynamic risk assessment, early-warning applications, and the optimization of eco-protection engineering in regulated reservoir environments, demonstrating broad applicability to other similar hydro-geotechnical coupled systems.

Acknowledgements This work was financially supported by the Ecological and Environmental Protection Fund of China Three Gorges Corporation (Grant No. NBWL202200369), the Scientific and Technological Research Project of the Department of Education of Hubei Province (Grant No. Q20231214), and the National Natural Science Foundation of China (Grant No. 52069016). The authors would like to express their sincere gratitude to the relevant funding organizations for their support in this research.

Author contribution ZiChao Shen: Writing - original draft. GuangXin Zhang: Methodology, Funding acquisition. LiWen Qiu: Investigation. GuiYun Huang: funding acquisition. Di Wu: Methodology, Resources. ShiJiang Zhu: Validation.

References

- [1]. Aleotti P, Chowdhury R (1999) Landslide hazard assessment: summary review and new perspectives. Bull Eng Geol Environ 58(1):21–44. https://doi.org/10.1007/s100640050066
- [2]. Bordoni M, Meisina C, Valentino R, et al (2020) From rainfall to slope failure: a probabilistic approach for shallow landslide triggering. Water 12(6):1774. https://doi.org/10.3390/w12061774
- [3]. Coppin NJ, Richards IG (eds) (1990) Use of vegetation in civil engineering. Construction Industry Research and Information Association (CIRIA), London.
- [4]. Demisa MG, Wang S, Hou Q, et al (2025) A probabilistic framework for rainfall-induced instability in unsaturated slopes using bivariate rainfall and multivariate soil random fields. Bull Eng Geol Environ 84(4):207. https://doi.org/10.1007/s10064-025-03654-4
- [5]. Gariano SL, Guzzetti F (2016) Landslides in a changing climate. Earth Sci Rev 162:227–252 https://doi.org/10.1016/j.earscirev.2016.08.011
- [6]. Ghestem M, Sidle RC, Stokes A (2011) The influence of plant root systems on subsurface flow: implications for slope stability. Bioscience 61(11):869–879. https://doi.org/10.1525/bio.2011.61.11.6
- [7]. Griffiths DV, Fenton GA (2004) Probabilistic slope stability analysis by finite elements. J Geotech Geoenviron Eng 130(5):507–518. https://doi.org/10.1061/(ASCE)1090-0241(2004)130:5(507)
- [8]. Guzzetti F, Peruccacci S, Rossi M, et al (2008) The rainfall intensity–duration control of shallow landslides and debris flows: an update. Landslides 5(1):3–17. https://doi.org/10.1007/s10346-007-0112-1
- [9]. Hou T, Xu G, Zhang D, et al (2022) Stability analysis of Gongjiacun landslide in the Three Gorges Reservoir area under the action of reservoir water level fluctuation and rainfall. Nat Hazards 114(2):1647–1683. https://doi.org/10.1007/s11069-022-05386-4
- [10]. Huang D, Song YX, Cui ZJ (2018) Triggering mechanism and mobility of the Huangtupo landslide in the Three Gorges Reservoir, China. Eng Geol 238:146–158. https://doi.org/10.1016/j.enggeo.2018.02.003
- [11]. Hutchinson JN (1977) Assessment of the effectiveness of corrective measures in relation to geological conditions and types of slope movement. Bull Int Assoc Eng Geol 16(1):131–155. https://doi.org/10.1007/BF02591467
- [12]. Ilstedt U, Malmer A, Verbeeten E, et al (2007) The effect of afforestation on water infiltration in the tropics: a systematic review and meta-analysis. For Ecol Manag 251(1–2):45–51. https://doi.org/10.1016/j.foreco.2007.06.014
- [13]. Jian W, Xu Q, Yin Y, et al (2018) Deformation and failure of a reservoir landslide under the combined effects of rainfall and water-level fluctuations: A case study of the Zhaoshuling landslide, China. Eng Geol 239:254–263. https://doi.org/10.1016/j.enggeo.2018.03.024
- [14]. Jian W, Yin Y, Xiao L (2014) Rate effect of reservoir water-level fluctuation on a bank landslide in the Three Gorges Reservoir. Landslides 11(2):265–275. https://doi.org/10.1007/s10346-012-0372-y
- [15]. Johnson MS, Lehmann J (2006) Double-funneling of trees: stemflow and root-induced preferential flow. Ecoscience 13(3):324–333. https://doi.org/10.2980/i1195-6860-13-3-324.1
- [16]. Liang W, Yang Y, Xu Z (2010) Laboratory study of the effects of plant roots on soil infiltration in a sandy loam soil. Hydrol Process 24(24):3538–3546. https://doi.org/10.1002/hyp.7777
- [17]. Liu X, Wang Y (2023) Analytical solutions for annual probability of slope failure induced by rainfall at a specific slope using bivariate distribution of rainfall intensity and duration. Eng Geol 313:106969. https://doi.org/10.1016/j.enggeo.2022.106969
- [18]. Mickovski SB, van Beek R, Salin F (2009) Uprooting resistance of vetiver grass (Vetiveria zizanioides) under different soil hydrological regimes. Plant Soil 324(1–2):147–160. https://doi.org/10.1007/s11104-009-9943-4
- [19]. Norris JE, Greenwood JR, van Beek LPH (2008) An integrated, process-based approach to assessing the effects of vegetation on slope stability. Nat Hazards Earth Syst Sci 8(4):873–888. https://doi.org/10.5194/nhess-8-873-2008
- [20]. Springman SM, Jommi C, Teysseire P (2003) Instability of steep slopes in unsaturated soils: case study of the Riella landslide. Geotechnique 53(1):3–19. https://doi.org/10.1680/geot.2003.53.1.3
- [21]. Stokes A, Atger C, Bengough A, et al (2009) Desirable plant root traits for protecting natural and engineered slopes. Plant Soil 324(1–2):1–30. https://doi.org/10.1007/s11104-009-0159-y
- [22]. Stokes A, Norris JE, van Beek R, et al (2008) Ecological mitigation of hillslope instability: ten key issues facing researchers and practitioners. Plant Soil 304(1–2):1–20. https://doi.org/10.1007/s11104-007-9546-y
- [23]. Take WA, Beddoe RA (2014) Recent advances in the understanding of rainfall-induced shallow landslides in partially saturated soil. Can Geotech J 51(9):973–993. https://doi.org/10.1139/egj-2013-0112
- [24]. Waldron LJ (1977) The shear resistance of root-permeated soil. Soil Sci Soc Am J 41(5):843–849. https://doi.org/10.2136/sssaj1977.03615995004100050005x
- [25]. Wang T, Liu Y, Wang J, et al (2020) Assessment of spatial variability of hydraulic conductivity of seasonally frozen ground in Northeast China. Eng Geol 274:105741. https://doi.org/10.1016/j.enggeo.2020.105741
- [26]. Zhang F, Deng M, Yi Q, et al (2022) Deformation characteristics and thresholds of the Tanjiawan landslide in the Three Gorges Reservoir Area, China. J Mt Sci 19(5):1370–1385. https://doi.org/10.1007/s11629-021-6982-4
- [27]. Zhang J, Han Z, Liu W, et al (2021) Spatiotemporal patterns of storm-induced landslides in the Three Gorges Reservoir area, China. Geomorphology 375:107545. https://doi.org/10.1016/j.geomorph.2020.107545
- [28]. Zhang Y, Hu X, Tannant DD, et al (2018) Field monitoring and deformation characteristics of a landslide with piles in the Three Gorges Reservoir area. Landslides 15(3):581–592. https://doi.org/10.1007/s10346-017-0910-2
- [29]. Zhao N, Hu B, Yi Q, et al (2017) The coupling effect of rainfall and reservoir water level decline on the Baijiabao landslide in the Three Gorges Reservoir Area, China. Geofluids 2017:3724867. https://doi.org/10.1155/2017/3724867